

# A Steerable Needle Technology Using Curved Concentric Tubes

Patrick Sears and Pierre Dupont

*Department of Aerospace and Mechanical Engineering*

*Boston University*

*110 Cummington Street, Boston, MA 02215, USA*

*{patsears|pierre}@bu.edu*

**Abstract** – A new approach to steerable needle design is proposed for use in minimally invasive surgery. The technology is based on sets of curved concentric tubes. By rotating and extending the tubes with respect to each other, the position and orientation of the needle tip, as well as the shape of the inserted length, can be controlled. A mechanics model is presented for computing the shape of the needle. Forward and inverse kinematic equations are also derived. In addition, experimental results are presented as validation of the approach.

**Index Terms** – *needle steering, minimally-invasive surgery.*

## I. INTRODUCTION

Percutaneous needle-based procedures are employed throughout the body for a broad variety of applications. In many cases, the need arises to steer along three-dimensional curves around bony or sensitive structures. In order to achieve minimal damage to tissue along the needle's insertion path as well as to maintain steering control inside fluid-filled body cavities, it is advantageous for a steerable needle to generate its own steering forces rather than relying on reaction forces from the surrounding tissue.

Examples in which steering around bony structures is needed include regional anesthesia for major joint reconstruction and epidural steroid injection for chronic pain management. Examples for which both the ability to steer and the avoidance of off-axis steering forces are critical arise in neurosurgery for tumor ablation and brachytherapy. The need to steer inside a body cavity arises in the navigation and articulation of interventional tools in minimally invasive intracardiac reconstructive surgery and arrhythmia management.

In current practice, the steering of straight flexible needles is accomplished by applying lateral forces at the base or tip. These forces cause the partially-inserted needle to flex in the desired steering direction. Base steering is accomplished by lateral displacement or rotation of the uninserted portion of the needle. Tip steering is accomplished using either a beveled or curved tip, both of which produce a lateral steering force in the direction of the bevel or curve. The steering direction is adjusted by rotating the needle about its axis. Since the needle is initially straight, both base and tip steering methods rely on tissue reaction forces to flex the needle along a curved insertion path. Success depends on the skill of the clinician,

the tissue properties (since they determine the steering force) and the complexity of the desired curve.

In the last five years, the robotics community has proposed methods for substantially improving needle steering through path planning [1],[2],[4]; steering automation [3],[5],[7],[8],[10] and needle technology [5],[8]. For steering, these techniques employ needle base motion [3],[4],[7],[8], bevel tip orientation [1][2][10] and variable curvature of the needle tip [5]. An alternate approach involving bending of the entire needle appears in [8].

Steering techniques that rely on tissue reaction forces to bend the needle possess the following shortcomings. First, small steering radii of curvature require the needle to be very flexible in bending with respect to the tissue. Flexibility in bending leads to problems of buckling during insertion as well as to excess torsional flexibility, which can also lead to loss of steering control. In addition, for a given needle, steering ability declines with decreasing tissue modulus. In the limit of zero tissue modulus (e.g., inside a fluid-filled body cavity) steering control is lost.

This paper presents a needle technology based on curved concentric tubes. The advantage of this approach is that such a needle can generate its own bending forces without relying on tissue reaction forces for steering. This enables high-curvature steering in all tissue types, i.e., from muscle to brain to body cavities, while minimizing damage to adjacent sensitive tissue which could arise from using tissue forces to flex the needle.

The paper is arranged as follows. The next section presents the proposed needle technology and a simple mechanics model for computing the shape of concentric curved tubes. Section III describes the kinematic equations and illustrates insertion path planning by means of several simple inverse kinematics examples. Section IV describes a prototype and evaluates the mechanics model by means of a calibration experiment. The final section presents conclusions.

## II. NEEDLE DESIGN

The fundamental problem of steering needles along complex curves while applying minimum off-axis force is that needles must be pushed at the proximal end rather than pulled at the distal end. If distal-end pulling was possible, the needle shaft could be made extremely flexible such that each section of the shaft would trace out the curve of the section in front of it in "follow the leader" fashion. To accomplish this while pushing

a stiff needle, the approach taken here is to extend the tip of the needle in telescoping fashion along paths of piecewise constant curvature.

During insertion, tissue deformation and needle compliance may necessitate midcourse path corrections. Such corrections can be achieved by adjusting the curvature of those sections of the needle comprised of balanced stiffness tube pairs (described below). While such adjustments may apply lateral forces to the tissue, their magnitude is likely to be substantially less than what would be required to bend the needle along this path adjustment.

#### A. Curved Concentric Tube Needles

Concentric curved tubes can be used to construct needles of piecewise constant curvature as well as of more general shapes. Only the former will be considered here owing to their greater clinical relevance as well as to their greatly reduced modeling complexity.

When curved tubes are inserted inside each other to form a needle, their common axis must conform to a mutual resultant curvature. By performing relative translations and rotations of the tubes, both the curvature as well as the overall length of the needle can be varied. Two limiting cases can be characterized by the interaction of a pair of tubes when (1) the bending stiffness of one tube is much larger than that of the other and (2) when their bending stiffnesses are approximately equal. These two cases are referred to as dominating stiffness and balanced stiffness tube pairs, respectively. While idealizations, this classification is useful since needle designs composed of an arbitrary number of tubes can be viewed as a combination of these two types of tube pairs. Each is described below.

1) *Dominating Stiffness Tube Pair*: Since the bending stiffness of one tube is much larger than that of the other, the pair of concentric tubes conforms to the curvature of the stiffer tube. When the more flexible tube is translated such that it extends beyond the end of the stiff tube, the extended portion relaxes to its original curvature. This is illustrated in Fig. 1 for the case of a stiff, straight outer tube and a curved inner flexible tube. As shown in Fig. 1(b), once the flexible tube is extended, the pair has two independent degrees of freedom associated with relative translation and relative rotation of the tubes. Tube pairs of this type have previously been used for tip steering of straight needles [5] and curved path insertion [6].

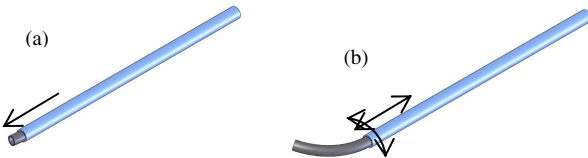


Fig. 1. Dominating stiffness tube pair. (a) When retracted, tubes conform to shape of stiff outer tube. (b) Portion of extended inner tube relaxes to its initial curvature.

2) *Balanced Stiffness Tube Pair*: Since the tubes are of similar stiffness, their unstressed curvatures interact to

determine their combined curvature. Relative rotation of the tubes causes the combined curvature to vary. An example is depicted in Fig. 2 in which the unstressed curvatures of the two tubes have been designed such that the pair is straight when the unstressed curvatures oppose each other and possesses maximum curvature when the individual curvatures are aligned. A second degree of freedom of the tube pair is associated with rotation of the pair about their base tangent. A balanced stiffness tube pair was first proposed in [8].

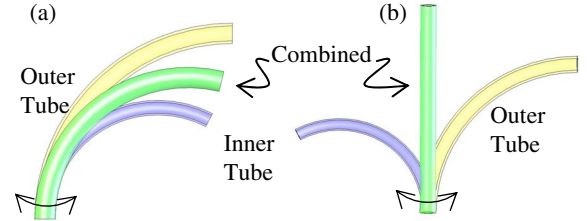


Fig. 2. Balanced stiffness tube pair. (a) Rotating tube pair with curvatures aligned, (b) Rotating tube pair with curvatures opposed.

#### B. Concentric Tube Curvature Model

The following analysis applies to an arbitrary number of concentric tubes. It is assumed that each tube has piecewise constant curvature and that bending stresses remain elastic. While the actual loading between tubes will consist of forces distributed along their common boundary, it is assumed here that each tube experiences pure bending. This approximation implies that the tubes apply bending moments to each other which are constant along their common length. These moments must be generated over negligibly short lengths at the ends of each constant curvature section. Finally, it is assumed that the tubes can be approximated as rigid in torsion.

Combining these assumptions with the Euler-Bernoulli beam model permits direct calculation of the resulting curvature of each length of a needle in which the individual tubes have constant curvature. In this way, tubes of piecewise constant curvature combine to form needles of piecewise constant curvature whose shape can be computed without resorting to integral equations.

The tubes are labeled with subscript indices,  $i = 1, 2, \dots, n$ , where 1 is the outermost tube and  $n$  is the innermost tube. As shown in Fig. 3, a coordinate frame can be defined as a function of arc length  $s$  along tube  $i$  by defining a single frame at the insertion point,  $F_i(0)$ , such that its  $z$  axis is tangent to the tube's centerline. The frame,  $F_i(s)$ , is obtained by sliding  $F_i(0)$  along the tube centerline without rotation about its  $z$  axis. Similarly, an insertion-point world frame,  $W(0)$ , is used to define a needle frame,  $W(s)$ , as a function of arc length. (See Fig. 4.) Superscripts will be used to indicate the coordinate frame of vectors and transforms.

Since the tubes are assumed rigid in torsion, any relative rotation between the tubes will be constant along their entire length. As the  $i^{\text{th}}$  tube's coordinate frame  $F_i(s)$  slides down its centerline, it experiences a body-frame angular rate of change per unit arc length given by

$$\bar{u}_i^{F_i(s)}(s) = \begin{bmatrix} \bar{\kappa}_{ix} & \bar{\kappa}_{iy} & \tau_i \end{bmatrix}^T, \quad (1)$$

in which  $(\bar{\kappa}_{ix}, \bar{\kappa}_{iy})$  are the  $x$  and  $y$  components of curvature due to bending and  $\tau_i = 0$  is the torsion. The over bars in (1) indicate values for the initial curvatures of the tubes before they are assembled. In the examples of Fig. 3, the tubes have nonzero  $y$  components of curvature in local frames,  $F_i(s)$ .

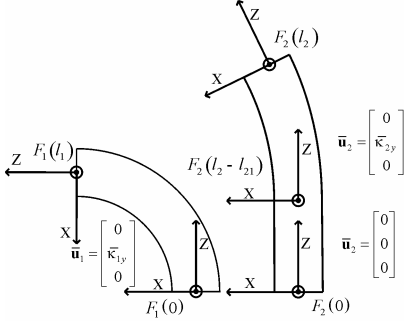


Fig. 3. Tube coordinate frames and initial curvatures.

When the tubes are assembled concentrically, the moment vector at any point along tube  $i$  is given by

$$m_i^{F_i(s)}(s) = K_i \left( u_i^{F_i(s)}(s) - \bar{u}_i^{F_i(s)}(s) \right) \quad (2)$$

in which  $m_i^{F_i(s)}(s)$  is the moment vector,  $u_i^{F_i(s)}(s)$  and  $\bar{u}_i^{F_i(s)}(s)$  are the resultant and initial angular frame rates and  $K_i$  is the frame-invariant stiffness tensor for a tube given by

$$K_i = \begin{bmatrix} E_i I_i & 0 & 0 \\ 0 & E_i I_i & 0 \\ 0 & 0 & J_i G_i \end{bmatrix}. \quad (3)$$

in which  $E_i$  is the modulus of elasticity,  $I_i$  is the area moment of inertia and  $G_i$  is the shear modulus. For tubes, the area moment of inertia is given by

$$I_i = (\pi/64)(d_o^4 - d_i^4) \quad (4)$$

in which  $d_i$  and  $d_o$  are the inner and outer diameters of the cross section. The maximum bending strain in a tube section subject to pure bending (constant bending moment and curvature) is given by

$$\varepsilon_{\max} = r_o \left\| \left( \kappa_{ix} - \bar{\kappa}_{ix} \right)^{F_i(s)}, \left( \kappa_{iy} - \bar{\kappa}_{iy} \right)^{F_i(s)} \right\| \quad (5)$$

While (2) applies on a point-wise basis, the pure bending assumption permits it to be applied to sections of the needle in which each tube has constant initial curvature. The moment equilibrium equation can be applied to each of these sections by transforming (2) for each tube to the needle frame,  $W(s)$ . Defining  $\theta_i$  as the  $z$  axis rotation angle from frame  $W(s)$  to frame  $F_i(s)$ , the curvature vectors transform as

$$\bar{u}_i^{W(s)} = R(z, \theta_i) \bar{u}_i^{F_i}. \quad (6)$$

in which  $R(z, \theta_i)$  is the rotation matrix. The moment equilibrium equation for the concentric tubes is

$$\sum_{i=1}^n m_i^{W(s)} = 0. \quad (7)$$

Since all tubes must conform the same final curvature,  $u_f^{W(s)}$ ,

$$u_f^{W(s)} = u_1^{W(s)} = u_2^{W(s)} = \dots = u_n^{W(s)} \quad (8)$$

Combining (2)-(8) yields an expression for the resultant angular frame rate for a section of needle length comprised of  $n$  overlapping tubes of constant curvature,

$$u_f^{W(s)} = \left( \sum_{i=1}^n K_i \right)^{-1} \sum_{i=1}^n K_i \bar{u}_i^{W(s)}. \quad (9)$$

Owing to the assumption of torsional rigidity, this expression takes the form  $u_f^{W(s)} = \begin{bmatrix} \kappa_{fx} & \kappa_{fy} & 0 \end{bmatrix}^T$ . The total moment applied to one tube by all the others can be interpreted as the vector sum of two bending moments - the moment necessary to remove its initial curvature  $\bar{u}_i^{W(s)}$  and the moment necessary to produce its final curvature  $u_f^{W(s)}$ .

### III. KINEMATICS

Neglecting rigid body displacements, the needle's degrees of freedom are those associated with each tube's insertion along, and rotation about, the common insertion point tangent. For a needle with  $n$  tubes, these comprise the  $2n$  kinematic variables. If six of these variables are independent, the needle tip can be arbitrarily positioned and oriented without insertion point pivoting or lateral displacement. If the manipulator possesses more than six independent variables then the shape of the needle along the insertion length can also be controlled resulting in multiple nominal insertion paths.

The tube shapes treated here are of piecewise constant curvature. To compute the overall shape of the needle, its inserted length is divided into sections such that each tube in that section has constant curvature. Applying the pure bending assumption independently to each section, its resultant curvature can be computed. Continuity between sections permits the computation of the configuration along the entire length of the needle.

As an example, the design of Fig. 4 consists of four concentric tubes extending from a straight rigid cannula. Tube dimensions are given in Table 1. Tubes 1 and 2 form a balanced stiffness pair and produce most of the lateral displacement of the needle tip. Tube 3 is much more flexible than the combination of tubes 1 and 2 and so the three tubes act together as a dominating stiffness tube pair. With a small radius of curvature at its distal end, tube 3 controls orientation of the needle tip. Tube 4 is most flexible and acts as a retraction-activated pair of forceps.

As shown in the table, tubes 1, 2 and 4 have constant curvature over their entire length. Tube 3 has finite curvature over a length of  $l_{31} = 4.71$  cm at its tip and zero curvature over the remainder of its length.

The kinematic variables can be defined using the coordinate frames introduced in section IIB. The angular kinematic variable for tube  $i$  is defined as  $\theta_i$ , the rotation angle about the  $z$ -axis between world frame  $W(s)$  and tube frame  $F_i(s)$ . The total inserted length of tube  $i$  measured from frame  $W(0)$  is denoted  $l_i$ . For tubes with multiple curvatures along their length,  $l_{ij}$  is used to denote the length of tube  $i$ 's  $j^{\text{th}}$  curved section, where  $j = 1$  corresponds to the distal end. This applies only to tube 3 in Table 1.

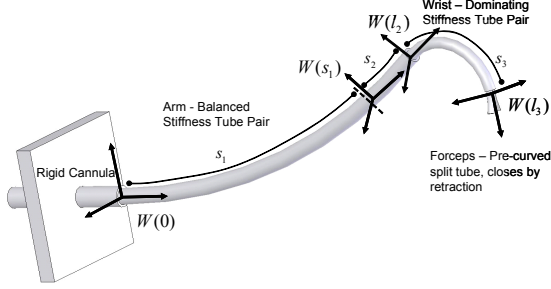


Fig. 4. Four-tube needle design

Table 1. Prototype design parameters.

Tube	1	2	3	4
Outer Diameter, $d_o$ (mm)	1.684	1.295	1.003	0.8
Inner Diameter, $d_i$ (mm)	1.346	1.036	0.813	0.615
Radii of Curvature (cm)	$\rho_1 = 11.89$	$\rho_2 = 4.16$	$\rho_{31} = 1.5$ $(l_{31} = 4.71)$	$\rho_4 = \infty$
(section lengths (cm))	$(l_1 = 7.58)$	$(l_2 = 7.58)$	$\rho_{32} = \infty$ $(l_3 - l_{31} = 7.58)$	$(l_4 = 13.3)$

### A. Forward Kinematics

Since the needle has piecewise constant curvature, its kinematics can be decomposed into two mappings. The first maps the kinematic variables  $\{(\theta_1, l_1), \dots, (\theta_n, l_n)\}$  (assuming  $n$  tubes) to an ordered list  $\{(u_{f1}^{W(s)}, s_1), \dots, (u_{fm}^{W(s)}, s_m)\}$  of curvature vectors,  $u_{fi}^{W(s)}$ , and associated arc lengths,  $s_i$ . Here,  $m$  is the number of constant curvature sections. Note that while the frame  $W(s)$  is a function of arc length,  $s$ , the curvature vectors  $u_{fi}^{W(s)}$  are constant over the lengths  $s_i$ .

The second mapping uses  $\{(u_{f1}^{W(s)}, s_1), \dots, (u_{fm}^{W(s)}, s_m)\}$  to express the frames  $W(s)$ ,  $0 < s \leq l_n$  in frame  $W(0)$ . This decomposition is convenient since it places all details of the design and curvature model in the first mapping.

1) *Mapping Tube Variables to Curvatures and Arc Lengths*: This mapping will be explained in the context of the four-tube design of Fig. 4. It is assumed that the tube insertion lengths,  $l_i$ , satisfy the following expression,

$$l_1 = l_2 \leq l_3 \leq l_4. \quad (10)$$

This implies that the needle is inserted fully assembled and that tubes 3 and 4 obey a telescoping pattern of extension. This results in four sections of constant curvature with arc lengths  $s_1$  to  $s_4$ , as labeled in Fig. 4. These lengths and the tubes to which they apply are

$$\begin{aligned} s_1 &= \max\{0, l_3 - l_{31}\}, & \text{tubes 1-4} \\ s_2 &= l_2 - s_1, & \text{tubes 1-4} \\ s_3 &= l_3 - l_2, & \text{tubes 3, 4} \\ s_4 &= l_4 - l_3, & \text{tube 4} \end{aligned} \quad (11)$$

Equations (6) and (9) can be applied to each needle section in (11) to solve for the curvatures  $u_{f1}^{W(s)}, \dots, u_{f4}^{W(s)}$ .

2) *Mapping Curvatures and Arc Lengths to Needle Coordinates*: This mapping applies to any needle of piecewise constant curvature. The needle coordinate frame  $W(s)$  can be written in terms of the insertion-point world frame  $W(0)$  as a concatenation of transformations. In particular, the needle tip frame is given by

$$W^{W(0)}(l_n) = T(u_{f1}^{W(s)}, s_1) \cdots T(u_{fm}^{W(s)}, s_m) \quad (12)$$

Each transformation,  $T(u_{fi}^{W(s)}, s_j)$ , can be computed as the matrix exponential of a twist with respect to arc length,

$$[v^T, \omega^T]^T = \left[ \begin{bmatrix} 0 & 0 & 1 \end{bmatrix}^T, u^T \right]^T / \|u\| \quad (13)$$

of magnitude  $s\|u\|$  [9]. This results in  $T(u, s) =$

$$\begin{cases} \begin{bmatrix} \frac{\kappa_x^2 + \kappa_y^2 \cos(s\|u\|)}{\|u\|^2} & \frac{\kappa_x \kappa_y (1 - \cos(s\|u\|))}{\|u\|^2} & \frac{\kappa_y \sin(s\|u\|)}{\|u\|} & \frac{\kappa_x (1 - \cos(s\|u\|))}{\|u\|^2} \\ \frac{\kappa_x \kappa_y (1 - \cos(s\|u\|))}{\|u\|^2} & \frac{\kappa_x^2 + \kappa_y^2 \cos(s\|u\|)}{\|u\|^2} & -\frac{\kappa_x \sin(s\|u\|)}{\|u\|} & -\frac{\kappa_y (1 - \cos(s\|u\|))}{\|u\|^2} \\ \frac{\kappa_y \sin(s\|u\|)}{\|u\|} & -\frac{\kappa_x \sin(s\|u\|)}{\|u\|} & \cos(s\|u\|) & \frac{\sin(s\|u\|)}{\|u\|} \\ 0 & 0 & 0 & 1 \end{bmatrix}, & \|u\| \neq 0 \\ \begin{bmatrix} I & [0 & 0 & s]^T \\ 0 & 1 \end{bmatrix}, & \|u\| = 0 \end{cases} \quad (14)$$

### B. Inverse Kinematics

If the dominating stiffness tubes are assumed not to flex at all due to the more flexible tubes, the solution can be obtained in two steps following the decomposition described for the forward kinematics. In the first step, the inputs are the coordinates frames for the needle insertion point,  $W(0)$ , and the needle tip,  $W^{W(0)}(l_n)$ , along with a description of the tube pairs. The latter includes the number of constant curvature segments and whether the curvature of each segment is fixed (i.e., a dominating stiffness tube pair) or variable (i.e., a balanced stiffness tube pair). The output of this step is the ordered list of curvatures and arc lengths,  $\{(u_{f1}^{W(s)}, s_1), \dots, (u_{fm}^{W(s)}, s_m)\}$ .

The second step is to invert the curvature model (9) to obtain  $\{\theta_1, \dots, \theta_n\}$  from  $\{u_{f1}^{W(s)}, \dots, u_{fm}^{W(s)}\}$ . The map of (11) must also be inverted to solve for  $\{l_1, \dots, l_n\}$  from  $\{s_1, \dots, s_m\}$ .

Both steps are illustrated here for a three-tube needle design corresponding to Fig. 4 with the inner forceps tube omitted.

1) *Computing Curvatures and Arc Lengths*: Closed-form solutions can be derived for simple designs. Here, the mapping is presented for a three-tube design consisting, from base to tip, of a variable curvature arc length followed by a fixed curvature arc length. While solutions exist for arbitrary needle base and tip coordinate frames, only  $xz$  plane displacements of  $W^{W(0)}(l_n)$  from  $W(0)$  are treated here.

The components of the forward kinematic frame at the tip of the needle are given by the following,

$$W^{W(0)}(l_3) = \begin{bmatrix} w_x & w_y & w_z & w_0 \\ 0 & 0 & 0 & 1 \end{bmatrix} \quad (15)$$

All curvatures in this example lie in the  $y$  direction due to the planarity of the needle. For any tip configuration described by (15), two solutions exist. These correspond to the fixed curvature distal arc having either positive or negative curvature. That is,

$$u_{f_2}^{W(s)} = \begin{bmatrix} 0 & \pm \|\bar{u}_3\| & 0 \end{bmatrix}^T \quad (16)$$

The sign choice in (16) dictates the sign choice in the following equations (17)-(22) and (29). The curvature of the proximal arc, which is only nonzero in the  $y$  direction, is then

$$u_{f_1}^{W(s)} \Big|_y = 2 \frac{\|\bar{u}_3\| w_0 \Big|_x \pm (w_x \Big|_x - 1)}{\|\bar{u}_3\| \|w_0\|^2 \pm 2(w_0 \cdot w_x)}, \quad (17)$$

where  $w_i \Big|_j$  is the  $j$  component of vector  $w_i$ .

The length,  $s_1$ , of the variable curvature proximal arc is given by its arc angle,  $\varphi_1$ , divided by its curvature.

$$\varphi_1 = \text{atan2} \left( \|\bar{u}_3\| w_0 \Big|_z \pm w_x \Big|_z, \|\bar{u}_3\| / u_{f_1}^{W(s)} \Big|_y - \|\bar{u}_3\| w_0 \Big|_x \mp w_x \Big|_x \right) \quad (18)$$

$$s_1 = \varphi_1 / u_{f_1}^{W(s)} \Big|_y \quad (19)$$

The initial and final angles,  $\varphi_{2i}$  and  $\varphi_{2f}$ , of the constant curvature distal arc are given as follows.

$$\varphi_{2i} = \text{atan2} \left( \pm \sin(\varphi_1), \mp \cos(\varphi_1) \right) \quad (20)$$

$$\varphi_{2f} = \text{atan2} \left( \mp w_x \Big|_z, \mp w_x \Big|_x \right) \quad (21)$$

The arc angle of distal arc,  $\varphi_2$ , is then

$$\varphi_{2+} = \begin{cases} \left| \varphi_{2f} - \varphi_{2i} \right|, & \varphi_{2f} - \varphi_{2i} > 0 \\ 2\pi - \left| \varphi_{2f} - \varphi_{2i} \right|, & \varphi_{2f} - \varphi_{2i} < 0 \end{cases} \quad (22)$$

$$\varphi_{2-} = \begin{cases} 2\pi - \left| \varphi_{2f} - \varphi_{2i} \right|, & \varphi_{2f} - \varphi_{2i} > 0 \\ \left| \varphi_{2f} - \varphi_{2i} \right|, & \varphi_{2f} - \varphi_{2i} < 0 \end{cases}$$

The length of the constant radius distal arc,  $s_2$ , is given by its arc angle and curvature,

$$s_2 = \varphi_2 / \|\bar{u}_3\| \quad (23)$$

2) *Computing Tube Rotation Angles and Insertion Lengths*: Writing (9) in terms of the kinematic variables gives,

$$u_{f_1}^{W(s)} = \frac{1}{(I_1 + I_2 + I_3)} \begin{bmatrix} -(I_1 \|\bar{u}_1\| \sin \theta_1 + I_2 \|\bar{u}_2\| \sin \theta_2) \\ (I_1 \|\bar{u}_1\| \cos \theta_2 + I_2 \|\bar{u}_2\| \cos \theta_2) \\ 0 \end{bmatrix} \quad (24)$$

Taking the magnitude squared of each side of (24) results in the following relation.

$$c = \frac{(I_1 + I_2 + I_3) \|u_{f_1}\|^2 - (I_1 \|\bar{u}_1\|)^2 - (I_2 \|\bar{u}_2\|)^2}{2I_1 I_2 \|\bar{u}_1\| \|\bar{u}_2\|} \quad (25)$$

$$\theta_2 - \theta_1 = \text{atan2} \left( \pm \sqrt{1 - c^2}, c \right) \quad (26)$$

The two solutions of (26) allow for  $\theta_1$  to be positioned either clockwise or counterclockwise from  $\theta_2$  while retaining the same curvature magnitude. For the needle to remain in the  $xz$  plane, the curvature must be of the form

$$u_{f_1}^{W(s)} = \begin{bmatrix} 0 & u_{f_1}^{W(s)} \Big|_y & 0 \end{bmatrix}^T \quad (27)$$

Equating (24) and (27) yields the following result.

$$\theta_2 = \pm \cos^{-1} \left( \frac{(I_2 \|\bar{u}_2\|)^2 - (I_1 \|\bar{u}_1\|)^2 + ((I_1 + I_2 + I_3) u_{f_1}^{W(s)} \Big|_y)^2}{2I_2 (I_1 + I_2 + I_3) \|\bar{u}_2\| u_{f_1}^{W(s)} \Big|_y} \right) \quad (28)$$

Using the result from (28) with the corresponding sign choice in (26) defines  $\theta_1$ .

The rotation angle of tube 3 depends only on the sign choice of (16).

$$(\theta_{3+}, \theta_{3-}) = (0, \pi) \quad (29)$$

Finally, the extension lengths are computed for each tube. The mapping from extension lengths to arc lengths is given by the following,

$$(s_1, s_2) = (l_1, l_3 - l_1) \quad (30)$$

This relation has a trivial inverse of the following form.

$$(l_1, l_2, l_3) = (s_1, s_1, s_1 + s_2) \quad (31)$$

3) *Examples*: Two examples are presented here for the three-tube needle design. The first demonstrates the capability to plan insertion paths around sensitive or bony tissue while the second demonstrates needle steering inside a body cavity.

Fig. 5 depicts the needle insertion point on the left with the needle target marked by an  $\times$ . Tissue regions to be avoided are shaded. Three possible insertion paths comprised of two constant-curvature sections are shown. In each case, the needle can be steered to the target in two steps. First, all tubes are inserted together along the proximal darker curvature. The inner tube is then extended along its constant curvature to reach the target. To compensate for tissue deformation during insertion, the curvature of the proximal section can be varied as needed.

Fig. 6 depicts the three-tube needle entering a body cavity from the left. Since needle shape is controlled by rotation and insertion of the tubes, it is possible for the needle tip to trace a path on the inner surface of the body cavity. For the case depicted, the needle tip follows a path normal to the surface.

Such a task would be impossible using standard approaches to the steering of straight needles.

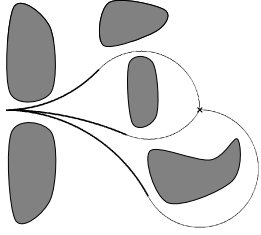


Fig. 5. Needle steering around bony or sensitive tissue.

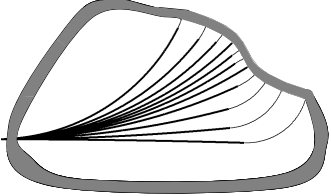


Fig. 6. Needle steering inside a body cavity.

#### IV. EXPERIMENTS

A four-tube prototype was constructed according to the design of Fig. 4. It is shown in Fig. 7 grasping a suture needle. Its curved nitinol tubes were shaped from straight tubes using a bake and quench process. As shown in Fig. 4, tube 4 acts as forceps. It was constructed by cutting its end with a wire EDM machine and heat setting the two fingers in a spread configuration. The gripper is closed by retracting the fingers into tube 3. At this time, the tubes have not been motorized to provide computer control of the kinematic variables. By manually controlling the tube rotation angles and insertion lengths, however, it is possible to grasp and manipulate objects with the needle.

To evaluate the accuracy of the curvature model presented in section IIB, the balanced stiffness tube pair (comprised of tubes 1 and 2 in Table 1) was tested as follows. The two tubes were mounted in bearings. Gears attached to each tube (one is shown in Fig. 7) permit the angle between the tubes to be manually set to an accuracy of  $\pm 1.5$  degrees. Images from a digital camera were used to estimate the curvature of the individual tubes as well as that of their concentric combination.



Fig. 7. Prototype steerable needle grasping a 4-0 suture needle.

Measurements of curvature as a function of relative angle of rotation permit evaluation of (9) and also provide a method for calibrating a specific tube pair. For a balanced stiffness tube pair, (9) can be written in terms of the magnitude and

direction of the curvature vector. The functional form of the squared magnitude facilitates curve fitting,

$$\|\kappa_f\|^2 = \alpha_1 + \alpha_2 \cos(\theta_2 - \theta_1) \quad (32)$$

Here,

$$\alpha_1 = \frac{(\|\bar{\kappa}_1\|I_1)^2 + (\|\bar{\kappa}_2\|I_2)^2}{(I_1 + I_2)^2}, \quad \alpha_2 = \frac{2\|\bar{\kappa}_1\|\|\bar{\kappa}_2\|I_1I_2}{(I_1 + I_2)^2} \quad (33)$$

The following experiment addresses two questions about the magnitude of curvature. First, it tests whether or not the concentric tubes have constant curvature over their length as the tubes are rotated with respect to each other. Second, it determines the accuracy of the fit given by (32).

##### A. Experimental Procedure

A Canon Power Shot A80 camera was used to photograph the tubes which were mounted just above a flat level gridded surface to limit the effects of perspective. The camera was positioned at a focal length of 20 cm from the flat surface and leveled. Data was first collected for the individual tubes. The tubes were rotated until they were parallel to the flat surface and photographed. Next, the tube pair was assembled and its radius of curvature was measured by rotating the inner tube relative to the outer tube to achieve a desired relative angle. The tube pair was then rotated until it was parallel with the flat surface and photographed. Data was taken in 15 degree increments except in the neighborhood of 180 degrees where it was taken in 3 degree increments. To check for asymmetry (e.g., due to finite rigidity in torsion), the tubes were rotated through 360 degrees in both the clockwise and counterclockwise directions.

##### B. Image Processing

Using the gridded surface under the tubes, a fourth-order radial shift was fit to eliminate error due to barrel distortion and the resolution of the images was found to be 132 pixels per cm. This characterization of the lens was used to transform the distorted data to rectilinear coordinates. Tube images were color thresholded to remove the grid and so retain only pixels composing the tubes. Radius of curvature was first estimated using a linear least squares fit to the  $n$  tube pixel coordinates,

$$x_i^2 + y_i^2 = \beta_1 x_i + \beta_2 y_i + \beta_3, \quad i = 1, \dots, n \quad (34)$$

where  $\beta_1 = -2x_c$ ,  $\beta_2 = -2y_c$ ,  $\beta_3 = x_c^2 + y_c^2 - r^2$ ,  $(x_c, y_c)$  are the coordinates of the center and  $r$  is the radius. This estimate was used to initialize a geometric fit using the Gauss-Newton nonlinear least squares method applied to minimizing

$$\sum_{i=1}^n (\|(x_i, y_i) - (x_c, y_c)\| - r)^2.$$

##### C. Results

The radii of tubes 1 and 2 were estimated as  $14.36 \pm 0.017$  cm and  $5.06 \pm 0.029$  cm, respectively. These values are slightly larger than the design values in Table 1 of 11.89 cm and

4.16 cm. This is typical of the relaxation to a steady-state shape that nitinol exhibits during the first few post-processing loading cycles.

The concentric tubes were found to conform closely to curves of constant curvature. For rotation angles of  $0-360^\circ$ , the radius of curvature varied between 10.62 cm and 29.82 cm with a maximum standard deviation of 0.019 cm.

Since data collection was performed manually, a limited number of trials were conducted in which the relative tube angle was varied over  $360^\circ$  in both directions. Fig. 8 depicts one trial in each loading direction. There is good agreement between the data sets indicating symmetry with respect to direction of rotation. This suggests that the assumption of rigidity in torsion is justified for this pair of tubes.

A weighted best fit of (32) to the data is shown as the dotted red curve for which  $(\alpha_1, \alpha_2) = (5.63, 3.53) \times 10^{-3} \text{ cm}^{-2}$ .

The weighting was selected to minimize tip position error over all rotation angles (3.66 mm maximum tip error for the 7.58 cm length tubes). While (32) captures the overall shape of the data, a better fit is obtained by adding a squared cosine to the equation,

$$\|\kappa_f\|^2 = a_1 + a_2 \cos(\theta_2 - \theta_1) + a_3 \cos^2(\theta_2 - \theta_1). \quad (35)$$

The coefficients  $(a_1, a_2, a_3) = (6.41, 3.54, -1.52) \times 10^{-3} \text{ cm}^{-2}$  produce the solid blue curve shown in the figure and yield a maximum tip position error of 1.6 mm.

Several important conclusions can be drawn from these results. First, they confirm the assumption that the concentric combination of constant-curvature tubes produces a resulting curvature which is also constant. This validates the approach taken in section III to model the kinematics assuming piecewise constant curvature.

Second, the simple proposed curvature model provides an efficiently computed approximate solution which is likely to be adequate for error-based endpoint control. Alternately, detailed calibration models, e.g., (35), can be used to obtain more accurate solutions. The decomposition of the forward kinematics proposed in section IIIA facilitates the substitution of alternate curvature models.

## V. CONCLUSIONS

A new approach to steerable needle design has been proposed based on the concentric combination of curved tubes. With this approach, needles can generate their own steering forces rather than relying on tissue reaction forces. While the use of multiple concentric tubes can increase the overall diameter of the needle, the benefit of high-curvature steering independent of tissue stiffness is likely to prove beneficial in many medical applications.

The proposed approach is also quite general. Numerous application-specific needle designs can be assembled using sequential combinations of dominating-stiffness and balanced-stiffness tube pairs. The curvature and kinematic models described here apply to all designs in which the individual tubes have piecewise constant curvature. These designs are

particularly useful since they permit “follow-the-leader” steering by extending the needle along paths of piecewise constant curvature. The calibration experiment and successful manual operation of the prototype confirm the practicality of the approach.

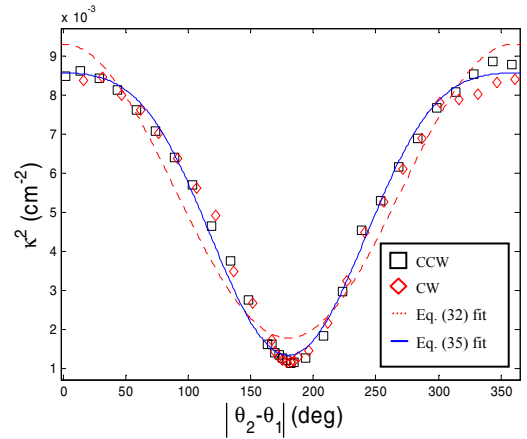


Fig. 8. Squared curvature versus relative tube angle.

## ACKNOWLEDGMENT

Thanks to James R. Rice for his helpful advice. Thanks also to Matt Heverly and Mark Salada for their assistance during the initial phase of this project. This research was funded by the NIH under Grant #R01 EB003052.

## REFERENCES

- [1] R. Alterovitz, A. Lim, K. Goldberg, G. S. Chirikjian, and A. M. Okamura, "Steering Flexible Needles Under Markov Motion Uncertainty," *IEEE/RSJ International Conference on Intelligent Robots and Systems*, 2005, pp. 120-125.
- [2] R. Alterovitz, K. Goldberg and A. Okamura, "Planning for Steerable Bevel-tip Needle Insertion Through 2D Soft Tissue with Obstacles," *IEEE Int. Conference on Robotics and Automation*, pp. 1652-57, 2005.
- [3] S. P. DiMaio and S. E. Salcudean, "Needle Insertion Modeling and Simulation," *IEEE Transactions on Robotics and Automation*, 19(5):864-875, 2003.
- [4] S.P. DiMaio and S.E. Salcudean, "Needle Steering and Model-based Trajectory Planning," *Medical Image Computing and Computer Assisted Intervention*, pp. 33-40, 2003.
- [5] R. Ebrahimi, S. Okzawa, R. Rohling, and S. E. Salcudean, "Handheld Steerable Needle Device," *Medical Image Computing and Computer Assisted Intervention*, pp. 223-230, 2003.
- [6] S. Gupta, HL Nguyen, FA Morello, K. Ahrar, MJ Wallace, DC Madoff, R. Murthy and ME Hicks, "Various Approaches for CT-guided Percutaneous Biopsy of Deep Pelvic Lesions: Anatomic and Technical Considerations," *RadioGraphics*, 24:175-189, 2004.
- [7] M. Loser and N. Navab, "A New Robotic System for Visually Controlled Percutaneous Interventions under CT Fluoroscopy", *Medical Image Computing and Computer-Assisted Intervention*, 2000.
- [8] M. Loser, "A New Robotic System for Visually Controlled Percutaneous Interventions under X-ray Fluoroscopy or CT-imaging," Dr. Ing. Dissertation, Microsystems Technology, U. Freiburg, Germany, 2005.
- [9] R. Murray, Z. Li and S. Sastry, "A Mathematical Introduction to Robotic Manipulation," CRC Press: Boca Raton, Florida, 1994.
- [10] R.J. Webster III, N.J. Cowan, G. Chirikjian, and A.M. Okamura, "Nonholonomic Modeling of Needle Steering," *9th International Symposium on Experimental Robotics*, Singapore, 2004.